Thermal performance of lightweight steel framed wall: The importance of flanking thermal losses

**Paulo Santos[1], Cláudio Martins[1],
Luís Simões da Silva[1] and Luís Bragança[2]**

Abstract

The thermal performance of a modular lightweight steel framed wall was measured and calculated with three-dimensional finite element method model. The focus of this article is on the effect of flanking thermal losses. The calculated heat flux values varied from -22% (external surface) to $+50\%$ (internal surface) when flanking loss was set to 0 as a reference case, thermal transmittance equal to 0.30 W/(m²·K). Other critical parameters were the existence of fixing 'L'-shaped steel elements and the perimeter thermal insulation (10 cm XPS).

Keywords

Lightweight steel framing walls, thermal transmittance, flanking heat losses, experimental measurements, three-dimensional numerical assessment

Introduction

The use of lightweight steel framing (LSF) as a structural element in buildings has increased in recent years. Its various advantages (Murtinho et al., 2010; Santos et al., 2011a, 2011b, 2012) include high mechanical strength and lightweight, easy and rapid prefabrication and high potential for recycling and reuse.

[1]ISISE, Civil Engineering Department, University of Coimbra, Coimbra, Portugal

[2]Civil Engineering Department, School of Engineering, University of Minho, Guimarães, Portugal

Corresponding author:
Paulo Santos, Departamento de Engenharia Civil, Faculdade de Ciências e Tecnologia, Universidade de Coimbra, Rua Luís Reis Santos – Pólo II, 3030-788 Coimbra, Portugal.
Email: pfsantos@dec.uc.pt

Yet, the high thermal conductivity of steel can lead to thermal bridges unless protected by continuous thermal insulation. Thermal bridges may increase the energy consumption up to 30% and nullify energy savings due to the use of solar thermal collectors (Erhorn-Klutting and Erhorn, 2009). Moreover, thermal insulation plays a key role in the building lifecycle (Gervásio et al., 2010). Given the larger difference in thermal conductivity between the steel frames and other materials, the quantification of the thermal transmittance (U-value) in LSF structures is more difficult than in traditional construction brick walls (Kosny et al., 1994).

EN ISO 6946:2007 (2007) presents an analytical calculation method to assess the thermal transmittance of building elements, but only for building assemblies with thermally homogeneous layers. On the contrary, the American Society of Heating, Refrigerating and Air-Conditioning Engineers (ASHRAE, 1993) zone method can be used to calculate the R-value of an assembly when it contains high thermal conductivity elements, such as steel, in its cross-section. This method is a modification of the parallel path method, in which the wall is considered as several parallel heat flow paths of different conductance from surface to surface and an area-weighting factor. Kosny et al. (1994) improved the modified zone method, allowing for estimating the influence of the thermal bridge in the parallel path method.

More recently, Gorgolewski (2007) suggested a simplified method where the metal studs break the continuity of thermal insulation. This method is an adaptation of the approach established in the EN ISO 6946:2007 (2007) that includes various additional parameters (e.g. flange width, stud spacing and depth) to account for the overall thermal behaviour of the steel framed element.

On the other side, one can perform thermal transmittance testing using either the heat flow meter sensors (ASTM C1155-95, 2007; ISO 9869:1994, 1994) or calibrated hot box (ASTM C1363-11, 2011; GOST 26602.1-99, 1999; ISO 8990:1994, 1994). However, since the energy performance of materials and building assemblies are significantly affected by moisture and air flows, the traditional testing using calibrated boxes may need to be modified or other techniques may need to be used to determine the thermal performance. Bomberg and Thorsell (2008) proposed a new methodology including both testing and modelling to evaluate energy performance of building enclosures under field conditions. The proposed methodology takes into account the effect of thermal bridges (framing correction) as well as moisture and airflow effects. They applied this methodology to evaluate a few residential walls (Thorsell and Bomberg, 2008) as well as two steel-based commercial walls (Thorsell and Bomberg, 2011).

Infrared (IR) thermography is a complementary experimental technique that helps to locate thermal bridges and heat losses. For the heat flow meter method, this technique also identifies the best places for sensor placement to ensure a representative instrumentation distribution along the element of interest (ASTM C1046-95, 2007; ASTM C1155-95, 2007). Zalewski et al. (2010) also discussed the advantages and limitations of IR thermography.

Several advanced numerical computational methods are currently available, such as finite element analysis (FEA) and computational fluid dynamics (CFD). In

comparison with the experimental approach, these numerical models, when validated, enable optimisation of construction assemblies. To this end, the ISO 10211:2007 (2007) establishes the specifications to be followed when modelling thermal bridges in buildings and test cases to assess the precision of numerical algorithms to compute heat flows and surface temperatures for validating the calculation method.

This article examines the effect of flanking losses on the thermal transmittance. We describe wall composition, geometry, dimension, domain discretisation, boundary conditions and the modelling of air layers. Then, the calculations from finite element method (FEM) model are compared with the test results allowing us to use the model to evaluate the effects of changes in several design parameters.

Description of the wall

The modular wall comprises a steel structure containing galvanised, cold-formed steel studs with different cross-sectional shapes: 'C' (100 × 40 × 10 × 1), 'U' (75 × 40 × 10 × 1) and 'Z' (75 × 25 × 1). Each wall module is 1.2 m wide and 2.49 m high. Figure 1 shows the steel structure containing insulation between the steel profiles as well as in the external layer.
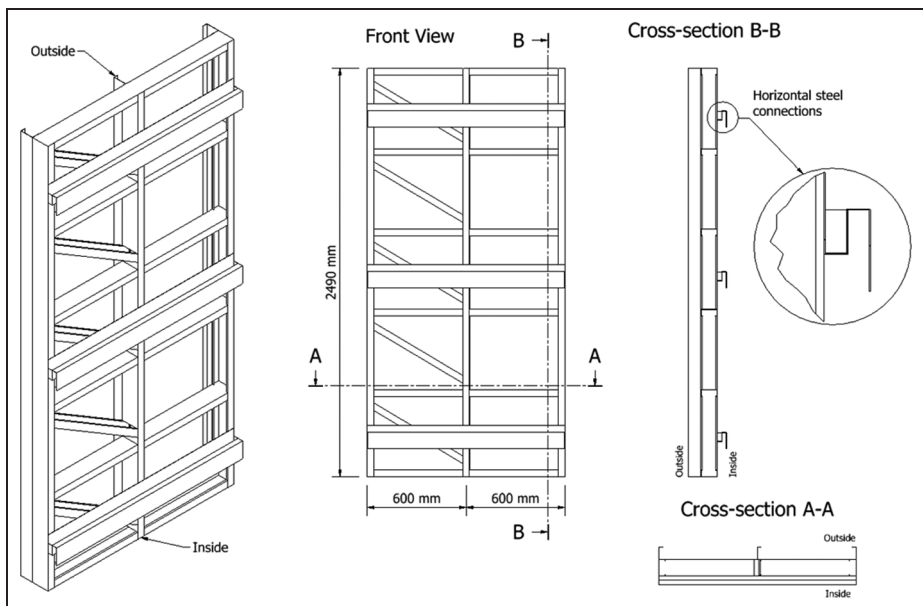

Figure 1. Steel structure of an LSF wall module.
LSF: lightweight steel framed.

Table 1. Wall materials and properties.

Material (from outer to inner surface)	Thickness (mm)	λ (W/(m·K))
Finish ETICS coat	4	0.75
EPS (ETICS insulation)	40	0.04
Windtight and water-resistant membrane	(Neglected in the computations)	
OSB	11	0.13
Stone wool	40	0.034
Air[a]	166	0.922
Steel frames (C100 × 40 × 10 × 1,	175	50
U75 × 40 × 10 × 1 and Z75 × 25 × 1)		
Stone wool	40	0.034
Wood	15	0.18
OSB	11	0.13
Plasterboard	13	0.25

[a]Solid equivalent thermal conductivity.
ETICS: external thermal insulation composite system; EPS: expanded polystyrene; OSB: oriented strand board.
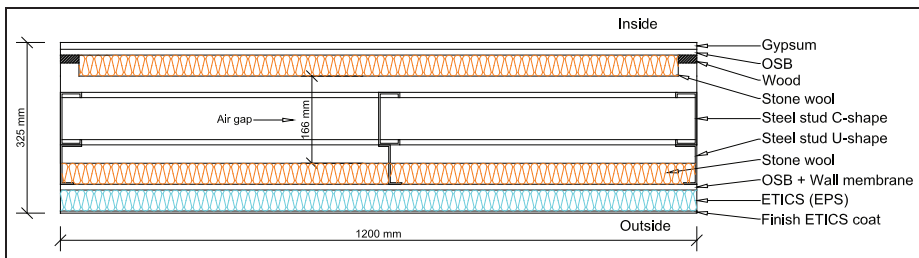
Figure 2. Horizontal cross-section of a wall module.
OSB: oriented strand board; ETICS: external thermal insulation composite system; EPS: expanded polystyrene.

This modular LSF wall contains external, fixed and interior detachable parts linked by three horizontal steel connections (see cross-section B-B of Figure 1 and Table 1). The wall has been examined: (a) before and (b) after the application of an external thermal insulation composite system (ETICS) with expanded polystyrene (EPS) (Figure 2).

Experimental approach

The temperature inside the test chamber was controlled by a split-type air conditioner, allowing the temperature to be set as high as 31°C. The gantry of test chamber was filled with three standard wall modules (1.20 m wide) and one smaller
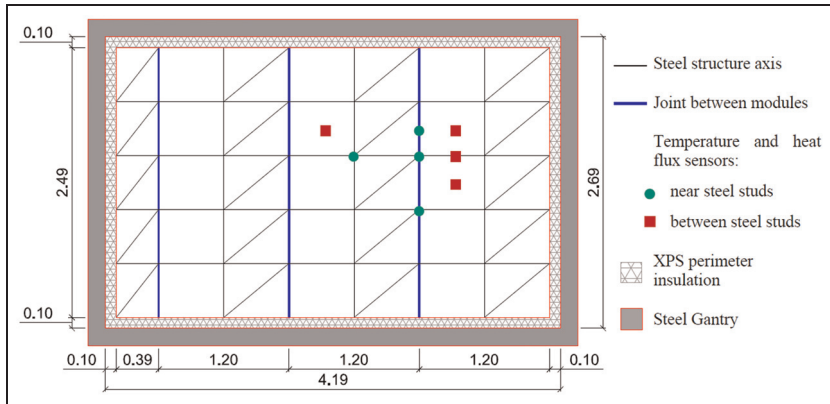
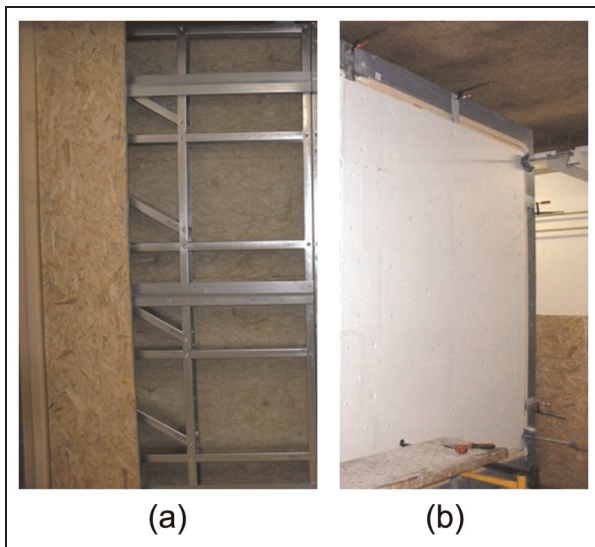**Figure 3.** Wall test specimen and mobile gantry.

Figure 4. Photographs of the wall module assembly: (a) inside view of the LSF wall structure and (b) external thermal insulation (EPS).
LSF: lightweight steel framed; EPS: expanded polystyrene.

module (0.39 m wide). To minimise the flanking heat losses, a continuous insulation layer of 10 cm XPS was placed between the wall modules and the steel gantry along its entire perimeter (Figure 3).

Figure 4(a) shows an interior view of the LSF wall structure in the gantry of the test chamber. Figure 4(b) displays the external thermal insulation (EPS) before the application of the finishing coating layer.
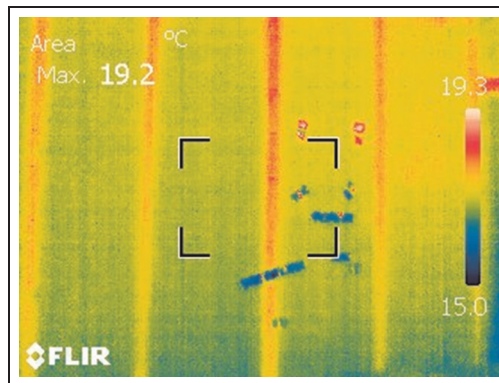
Figure 5. Infrared thermal image of the wall without ETICS.
ETICS: external thermal insulation composite system.

Experimental setup

The heat flux passing through each of the tested walls was monitored in certain key points (see Figure 3) using heat flux sensors (precision of ±5%). The surface temperatures were measured using PT100 surface temperature sensors with an accuracy of ±0.4°C. To measure the air temperature inside the wall air gap, a PT100 needle temperature sensor with the same precision as the surface temperature sensors was used. To monitor the ambient air temperature inside/outside of the test chamber, thermohygrometers (accuracy of ±3%) were used. All sensor measurements were registered in a data logger (Campbell Scientific CR1000) with a multiplexer (Campbell Scientific AM16/32B), reducing the number of communication channels required. The exception is the thermohygrometers, which have an incorporated data logger.

IR thermography

Figure 5 shows the temperature on the external surface of the wall measured with IR camera (FLIR Systems, ThermaCAM T400) before applying the external thermal insulation. The location of the vertical steel studs is visible. The horizontal and diagonal profiles are not visible because they are better insulated and have no direct contact with the external oriented strand board (OSB).

Measurements

Figure 6 shows an example of the measured temperatures obtained during the tests with ETICS. The internal mean ambient temperature is 30.8°C. The mean external ambient temperature is 18.4°C. The data sampling time interval of each sensor was 2 min. Figure 6(b) presents the recorded heat flux data, and the difference between
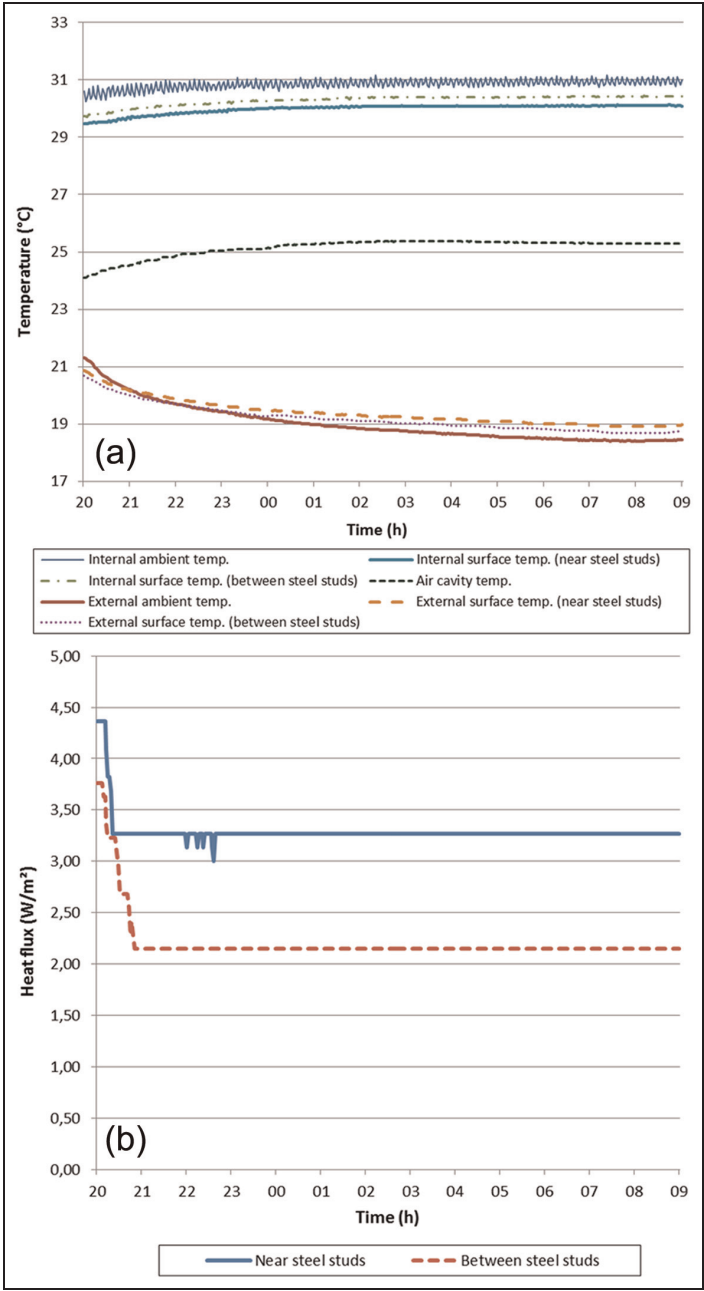
Figure 6. Example of recorded data (wall with ETICS): (a) temperature measurements and (b) heat flux measurements.

ETICS: external thermal insulation composite system.

Table 2. Thermal transmittance values: experimental approach.

Description	U-value (W/(m²·K))		
	Between steel frames	Near steel frames	Overall wall value
Without ETICS	0.219	0.767 (+250%)	0.40 (+84%)
With ETICS	0.178	0.279 (+57%)	0.21 (+20%)

ETICS: external thermal insulation composite system.

the two zones is approximately 1.1 W/m² (an increase of 50% is caused by the thermal bridges).

Thermal transmittance computation

Because these results (mean values) were obtained for steady-state conditions using a heat flow meter method, the computations were performed accordingly with the procedures presented in several standards for in situ measurements. The overall value for the wall is weighted in accordance with the area of influence of each sensor, which in turn was determined with ASHRAE zone method assisted by IR images (see Table 2).

Two sets of tests are presented: (a) the wall without the exterior thermal insulation system and (b) with ETICS comprising 40 mm of EPS. While the overall thermal transmittance of the wall is 84% higher than the measured U-value between the steel studs, adding the ETICS layer reduces the difference between the global wall U-value and that measured between the vertical steel studs to 20% and the U-value of the wall with ETICS is 0.21 W/(m²·K).

Numerical approach

Domain discretisation

ANSYS CFX finite element model of the LSF wall structure used 308,189 nodes (beyond which the results did not change after implementing further refinement).

Boundary conditions

For the interior T = 30.8°C and exterior T = 18.4°C, EN ISO 6946:2007 (2007) for horizontal heat flow (indoor conditions) recommends the film coefficient of 7.69 W/(m²·K).

Modelling air spaces

The air gap inside the wall was modelled as either (a) a still air layer or (b) fluid modelled with CFD.

Equivalent thermal conductivity. The EN ISO 6946:2007 (2007) presents a table of values with the equivalent thermal resistance for unventilated air gaps. A thermal resistance of 0.18 m^2·K/W is prescribed for an air layer with a thickness of 166 mm, assuming a horizontal heat flow. Using these values, an equivalent thermal conductivity of 0.922 W/(m·K) was obtained.

CFD. In this approach, the buoyancy model was selected for convection and the Monte Carlo model for radiation. The air thermal conductivity used was 0.0261 W/(m·K). The CFD and still air layer give similar results, with the overall thermal transmittance difference between them being 0.0046 W/(m^2·K).

Validation of the three-dimensional FEM model

Detailed complete three-dimensional model

To reproduce the experimental conditions of the wall, the FEM model had to include not only the steel structures but also materials surrounding perimeter of the wall included an XPS insulation layer, the 'L'-shaped steel fixing elements and the steel gantry. The three-dimensional (3D) model yielded an overall thermal transmittance of 0.235 W/(m^2·K). This value, although slightly higher than the experimental value (0.214 W/(m^2·K)), can be considered acceptable based on the uncertainties involved in the systems (e.g. precision of the heat flux sensor being ±5% and quantification of the steel stud influence zone).

Simplified models

To further evaluate the FEM model, two additional comparative analyses were performed with the wall module to compare the results with a two-dimensional (2D) THERM software and with the analytical expression for homogeneous layers (Table 3).

For the comparative, simplified wall (without any steel frame), all three models (analytical, THERM and ANSYS) gave the same U-value: 0.249 W/(m^2 K). For

Table 3. Verification results of the 3D FEM model.

Model description		U-value (W/(m^2·K))			
		Measured	3D FEM	2D FEM	Analytical
Detailed complete 3D FEM model		0.214	0.235	–	–
Only wall module	Without steel frames	–	0.249	0.249	0.249
	Only vertical steel studs	–	0.269	0.27	–

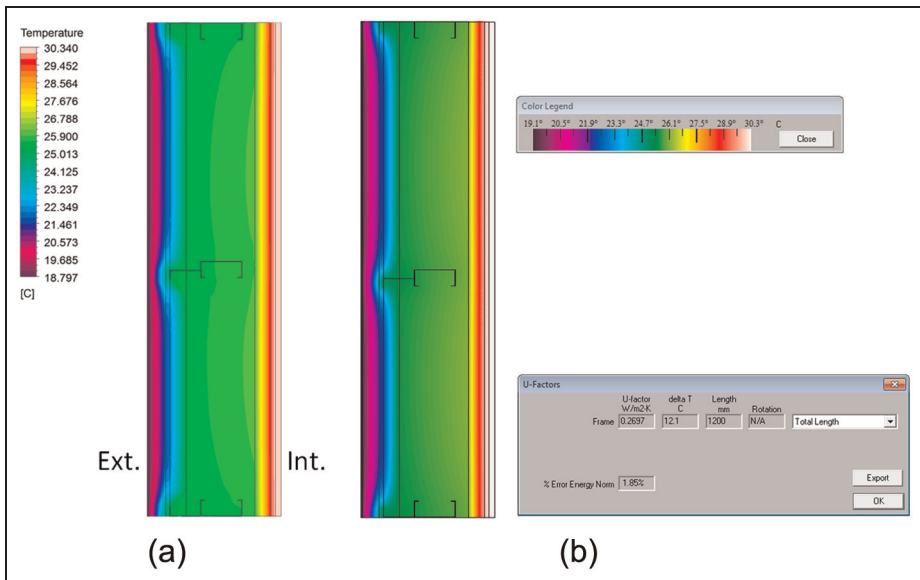3D: three-dimensional; FEM: finite element method.

Figure 7. Temperature distribution inside a horizontal cross-section module of the wall with ETICS: only vertical steel studs: (a) 3D FEM model – ANSYS CFX and (b) 2D FEM model – THERM.
ETICS: external thermal insulation composite system; 3D: three-dimensional; 2D: two-dimensional; FEM: finite element method.

wall with only vertical steel studs (enabling a 2D model), one obtained 0.270 and 0.269 W/(m²·K) for the 2D (THERM) and 3D (ANSYS) models, respectively.

Figure 7 illustrates the temperature distribution inside a horizontal cross-section of the wall in both models, showing again the good agreement between predictions, with slight differences near the steel stud outer flange.

IR thermography images

The measured and predicted surface temperatures were compared without ETICS. The results are similar. The visible difference between the measured and predicted surface temperatures is related to the buoyancy effect that is visible in the IR thermal images (Figure 5). This effect leads to higher values in the upper zone (Figure 8).

Parametric study

Several models, displayed in Table 4, modified the validated model (Model D) by removing parts, changing material properties and setting different boundary
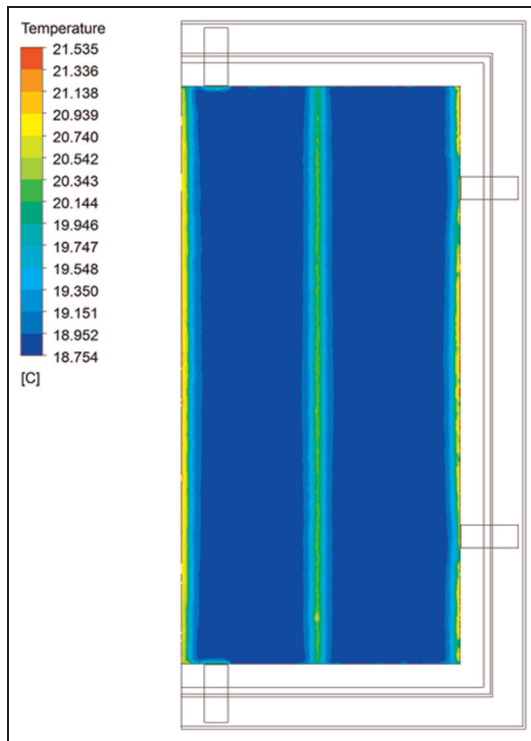
Figure 8. External surface temperatures predicted by the 3D FEM model: wall without ETICS.
ETICS: external thermal insulation composite system; 3D: three-dimensional; FEM: finite element method.

Table 4. Parametric study: overview of models and results.

Model	Model description					U-value (W/(m²·K)) (ΔU)	
	Adiabatic edges	'L'	XPS	Gantry		External[a]	Internal[a]
				Steel	Wood		
A	✔					0.301 (–)	0.301 (–)
B	✔	✔				0.264 (−12%)	0.355 (+18%)
C		✔	✔			0.236 (−22%)	0.449 (+49%)
D[b]		✔	✔	✔		0.235 (−22%)	0.452 (+50%)
E		✔	✔			0.245 (−19%)	0.425 (+41%)
F		✔			✔	0.247 (−18%)	0.421 (+40%)
G		✔	✔		✔	0.237 (−21%)	0.447 (+49%)

[a]Surface where the heat flux values were obtained.
[b]Model validated by comparison to experimental measurements (only external heat flux).

conditions (e.g. adiabatic edges). Thermal transmittance values are also shown for the reference case (Model A) with the zero flanking thermal loss (adiabatic edges) and two predicted U-values based on the heat flow values from the cold or hot surfaces.

No flanking losses

In this case (Model A), the predicted U-value is 0.301 W/(m^2·K) and the heat flux is identical on both surfaces, because there is no flanking loss (adiabatic edges). Therefore, the average heat flux value in each wall surface is equal. Note that this value is significantly higher than the measured one, 0.214 W/(m^2·K), proving the relevance of the flanking thermal conditions used in the experimental tests.

Figure 9 shows the heat flux and the surface temperature assuming no flanking heat losses (Model A). The effects of the vertical steel studs in the exterior surface (Figure 9(a)) and the horizontal steel connections in the internal surface of the wall (Figure 9(b)) are clear. Note that the negative heat flux values in the external side of the wall mean this wall surface is losing heat (cold surface).

With flanking losses

U-value: external surface heat flow. This section presents the thermal transmittance values obtained using the average external surface heat flow from 3D FEM model, displayed in Figure 10, for conditions presented in Table 4.

Model B is the Model A with the addition of the 'L'-shaped steel fixing elements used in the experimental tests. The wall perimeter is adiabatic, except for the salient part of the 'L' element and the ETICS, in which the exterior boundary conditions were imposed. These fixing elements led to a decrease in the U-value of 0.037 W/(m^2·K). This 12% reduction in the thermal transmittance value is caused by the lower heat flux perpendicular to the wall and the lateral heat flux to the steel fixing elements. Additionally, given that the thickness of the ETICS (40 mm) and finishing coating (4 mm) is salient to the supporting gantry, a geometric linear thermal bridge is clearly visible along the edge of the wall in Figure 10. Because the entire edge surface thickness was adiabatic in the previous model, this feature also increments the flanking heat loss, leading to a decrease in the U-value when the heat flux from the external wall surface is considered.

Model C introduces a 10-cm XPS insulation layer around the wall perimeter (the same insulation experimental conditions applied around the test specimen). The U-value was 0.028 W/(m^2·K) lower than those of Model A. This finding shows that the 10-cm-thick XPS insulation layer is not sufficient to avoid the flanking thermal losses, particularly when there are steel fixing plates. The lower heat flow (absolute value) through the wall is visible when comparing Figure 10(b) to (a).

Model D is the same model that was previously validated, having the same support conditions of the experimental tests, that is, a steel gantry, 10-cm XPS
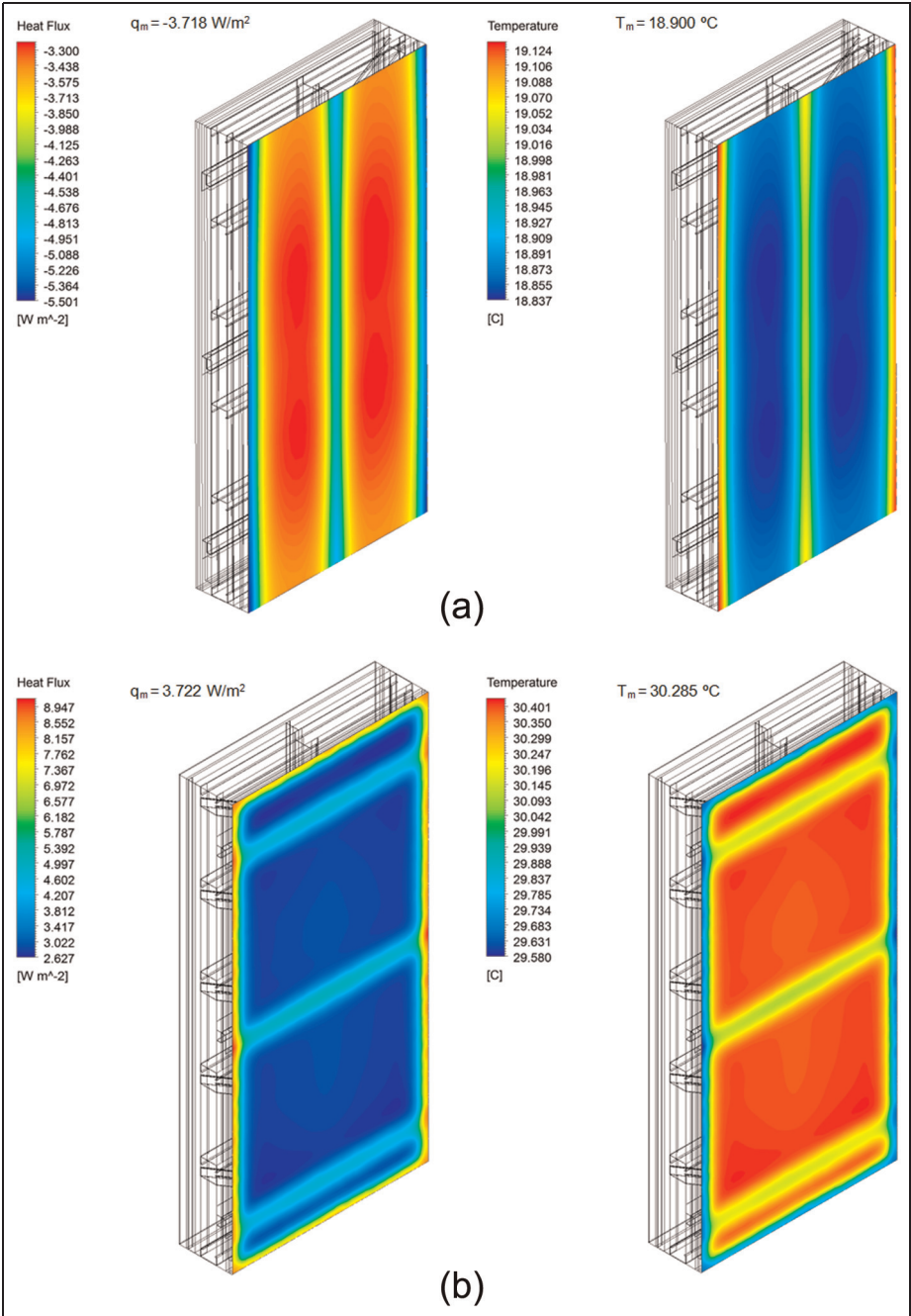
Figure 9. Heat flux and surface temperatures: Model A – adiabatic edges: (a) exterior view and (b) interior view.
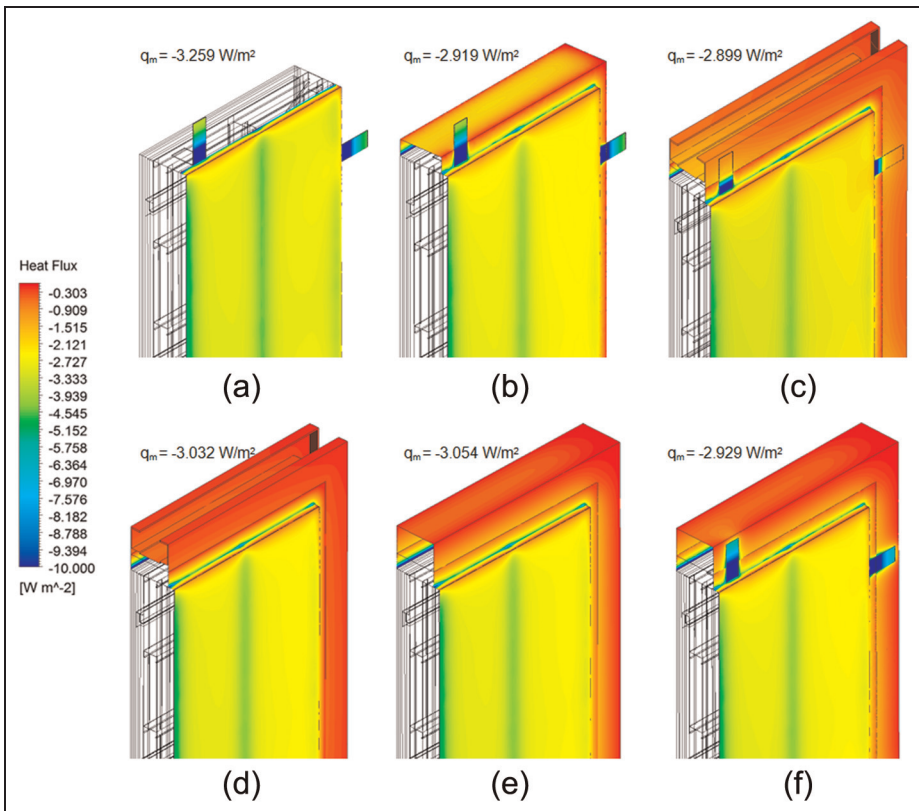
Figure 10. Heat flux: external surface view: (a) Model B: 'L' fixing elements, (b) Model C: 'L' + XPS edge insulation, (c) Model D: 'L' + XPS + steel gantry, (d) Model E: XPS + steel gantry, (e) Model F: XPS + wood gantry and (f) Model G: 'L' + XPS + wood gantry.

insulating layer along the perimeter and several 'L' fixing elements. Relative to the previous model, adding the steel gantry only decreased the U-value by 0.001 W/ ($m^2 \cdot K$), showing that the flanking heat flux is constrained by both the XPS insulating layer and 'L'-shaped steel fixing plates (Figure 10(c)).

Model E assumes that the wall specimens were fixed with polyurethane foam instead with the 'L' fixing element. The U-value increased slightly to 0.245 W/ ($m^2 \cdot K$), given the lower flanking thermal losses. Compared with the reference case (Model A), the decrease in the obtained U-value is now 19%.

The last two models (F and G) intend to evaluate the importance of the gantry material (wood instead of steel) in the obtained U-value of the LSF wall. When there are no fixing 'L'-shaped elements (Models E and F), the obtained U-values are similar, corresponding to a decrease of 19% and 18%, respectively. The relevance of the gantry material increases when steel fixing elements are included.
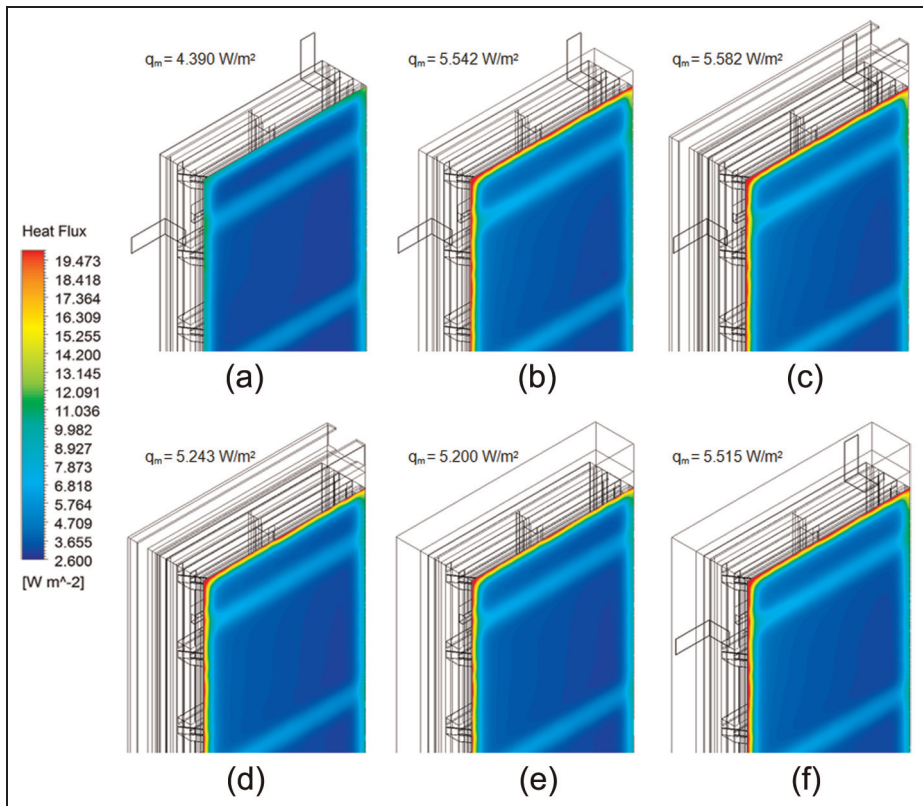
Figure 11. Heat flux: internal surface view: (a) Model B: 'L' fixing elements, (b) Model C: 'L' + XPS edge insulation, (c) Model D: 'L' + XPS + steel gantry, (d) Model E: XPS + steel gantry, (e) Model F: XPS + wood gantry and (f) Model G: 'L' + XPS + wood gantry.

In this case (Model G), the decrease in the U-value is higher (21%) and near the value obtained for Model D with steel gantry (22%).

U-value: internal surface heat flow. This subsection presents the results of the computation of the thermal transmittance value of the wall using the heat flow obtained along the inside surface of the wall (hot surface), displayed in Figure 11, for the same support conditions previously presented.

Heat losses from the wall perimeter lead to a higher heat flux in the hot (internal) surfaces, opposite to that observed earlier because the higher flanking transmission leads to lower heat flow values on the cold surfaces. Yet, the increase in the U-value is now much more pronounced (+ 50%) compared with the previous decrease in the U-values (−22%). The reason for this discrepancy is that the heat flow crossing the hot surface is divided into two parts: (a) perpendicular, towards the external surface of the wall (cold surface), and (b) lateral, towards the perimeter of the wall.

Let us analyse those differences. When the 'L' fixing elements are added to the adiabatic wall perimeter, the U-value difference in Model B is smaller (+ 18%) than when other measures are taken; Models C, D and G near + 50%. Finally, intermediate U-value differences occur in the remaining models (E and F), where there are no fixing elements (near + 40%). Regarding these three features, the only one that is clearly visible in Figure 11 is the first one, that is, the heat flux in the internal wall surface within Model B (Figure 11(a)) is clearly lower than all the others. The heat flux mean values, also displayed in Figure 11, confirm the previously mentioned sets of models.

Discussion

This research shows that depending on where the heat flux was measured, the thermal transmittance values could vary from -22% (external surface) to + 50% (internal surface), even though the wall had adiabatic edge surfaces, that is, had no flanking losses (the reference case).

Several parameters were examined, namely, fixing elements, perimeter thermal insulation, support gantry and material (steel or wood). The most impact gave the existence of 'L'-shaped fixing elements, which showed a U-value variation of -22% or + 50% (external or internal surfaces, respectively). The relevance of these fixing steel elements is decreased (-12% and + 18%) when the remaining wall surface perimeter is adiabatic.

When there were no steel fixing elements, the use of 10-cm XPS perimeter insulation is sufficient to reduce the flanking thermal losses of a steel gantry to values near those provided by a wood gantry. However, in comparison with an LSF with an adiabatic perimeter, the relevance of the flanking thermal loss remains high (-19%; + 41%). This study quantified how the flanking thermal losses may drastically change the measured global thermal transmittance of a building component (e.g. façade wall).

As shown in the parametric study, simple localised steel contacts in the periphery of the wall can provide considerable changes in the thermal transmittance value related to the increased flanking heat loss. Furthermore, in real buildings, there are always adjacent construction elements (e.g. walls, floors, roofs), where the structure is usually directly connected. Therefore, the significance of flanking heat losses could be even greater than the values herein obtained. Thus, the heat exchange with adjacent construction elements should also be considered when rating the energy efficiency of building elements.

Conclusion

The thermal performance of a modular LSF wall was examined with a focus on the impact of the flanking heat losses on the thermal transmittance of the wall. Performing an experimental evaluation of the FEM model and comparing it with

two additional models and IR thermography allowed the authors to use the 3D
FEM model for subsequent parametric study. The parametric study quantifies the
importance of flanking heat losses in the U-value of the LSF wall.

Several key parameters were identified, and its relative importance was quanti-
fied. One of the most important is to use an average of values measured on both
sides of the wall given that in practice the edges are always non-adiabatic.
Furthermore, the most relevant parameters were, by decreasing order, the support
steel gantry, the perimeter thermal insulation and the wall steel fixing elements.
Flanking heat loss must be taken into account, not only in laboratory tests or
numerical simulations but also in real buildings given the lateral heat exchange
with the adjacent construction.

Declaration of conflicting interests

Funding

References

American Society of Heating, Refrigerating and Air-Conditioning Engineers (ASHRAE)
(1993) *Handbook of Fundamentals*. Atlanta, GA: ASHRAE.
ASTM C1046-95 (2007) *Standard Practice for In-Situ Measurement of Heat Flux and
Temperature on Building Envelope Components*. West Conshohocken, PA: American
Society for Testing and Materials.
ASTM C1155-95 (2007) *Standard Practice for Determining Thermal Resistance of Building
Envelope Components from the In-Situ Data*. West Conshohocken, PA: American Society
for Testing and Materials.
ASTM C1363-11 (2011) *Standard Test Method for Thermal Performance of Building
Materials and Envelope Assemblies by Means of a Hot Box Apparatus*. West
Conshohocken, PA: American Society for Testing and Materials.
Bomberg M and Thorsell T (2008) Integrated methodology for evaluation of energy
performance of the building enclosures – part 1: test program development. *Journal of
Building Physics* 32(1): 33–48.
EN ISO 6946:2007 (2007) Building components and building elements – thermal resistance
and thermal transmittance – calculation method.
Erhorn-Klutting H and Erhorn H (2009) *ASIEPI – Impact of Thermal Bridges on the Energy
Performance of Buildings*. Stuttgart: Fraunhofer Institute for Building Physics.
Gervásio H, Santos P, Simões da Silva L, et al. (2010) Influence of thermal insulation on the
energy balance for cold-formed buildings. *International Journal of Advanced Steel
Construction* 6(2): 742–766.

Gorgolewski M (2007) Developing a simplified method of calculating U-values in light steel framing. *Building and Environment* 42: 230–236.

GOST 26602.1-99 (1999) Windows and doors. Methods of determination of resistance of thermal transmission. Interstate Standard of Russian Federation.

ISO 10211:2007 (2007) Thermal bridges in building construction – heat flows and surface temperatures – detailed calculations.

ISO 8990:1994 (1994) Thermal insulation – determination of steady-state thermal transmission properties – calibrated and guarded hot box.

ISO 9869:1994 (1994) Thermal insulation – building elements – in-situ measurement of thermal resistance and thermal transmittance.

Kosny J, Christian JE, Barbour E, et al. (1994) *Thermal performance of steel-framed walls.* CRADA Final Report ORNL93-0235, 21 November. Oak Ridge, TN: Oak Ridge National Laboratory.

Murtinho V, Ferreira H, Correia A, et al. (2010) Affordable houses: architectural concept of light steel residential house. In: *ICSA2010 – International conference on structures and architecture*, Guimarães, Portugal, 21–23 July 2010. London: Taylor & Francis Group, pp. 1291–1297, ISBN 978-0-415-49249-2.

Santos P, Gervásio H, Simões da Silva L, et al. (2011a) Influence of climate change on the energy efficiency of light-weight steel residential buildings. *Civil Engineering and Environmental Systems* 28: 325–352.

Santos P, Simões da Silva L and Ungureanu V (2012) *Energy Efficiency of Light-Weight Steel-Framed Buildings.* 1st ed. Lisbon: European Convention for Constructional Steelwork (ECCS), Technical Committee 14 – Sustainability & Eco-Efficiency of Steel Construction, ISBN 978-92-9147-105-8, N. 129.

Santos P, Simões da Silva L, Gervásio H, et al. (2011b) Parametric analysis of the thermal performance of light steel residential buildings in Csb climatic regions. *Journal of Building Physics* 35(1): 7–53.

Thorsell T and Bomberg M (2008) Integrated methodology for evaluation of energy performance of building enclosures: part 2 – examples of application to residential walls. *Journal of Building Physics* 32(1): 49–65.

Thorsell T and Bomberg M (2011) Integrated methodology for evaluation of energy performance of the building enclosures: part 3 – uncertainty in thermal measurements. *Journal of Building Physics* 35(1): 83–96.

Zalewski L, Lassue S, Rousse D, et al. (2010) Experimental and numerical characterization of thermal bridges in prefabricated building walls. *Energy Conversion and Management* 51(12): 2869–2877.